



Helical phase masks for controlling optical vortices: Necessary and sufficient conditions



Cristina M. Gómez-Sarabia^a, Luis M. Ledesma-Carrillo^b, Jorge Ojeda-Castañeda^{c,*}

^a Digital Arts, DICIS, University of Guanajuato, Salamanca, 36885, Mexico

^b Multi-Disciplinary Studies, University of Guanajuato, Yuriria, 36885, Mexico

^c Electronics Department, DICIS, University of Guanajuato, Salamanca, 36885, Mexico

ARTICLE INFO

Keywords:

Optical vortices
Phase-conjugate pairs
Optical switches
Optical alignment
Optical sensors

ABSTRACT

We identify the necessary and sufficient conditions for controlling the presence of optical vortices. Next, we unveil the use of two different pairs of transparent masks, which are useful for governing the presence of optical vortices. The elements of the first pair have quadratic helical variations. The elements of the second pair have cosinusoidal helical variations. In both cases, one element of the pair has a complex amplitude transmittance that is equal to the complex conjugate of the other element. By introducing an in-plane rotation, between the elements of a pair, one can control the presence of an optical vortex. We apply the previous results for detecting angular misalignments.

1. Introduction

For their inherent physical characteristics and for its potential uses, optical vortices have attracted the attention of several researches [1–10].

Helical modulations on Bessel beams have been used for linking the Eigensolutions of the scalar wave equation with the Montgomery's analysis of the self-imaging phenomenon [11,12].

As optical sensors and as imaging devices, helical phase variations are useful for setting a test for optical alignment [13], for implementing a coronagraph [14], for proposing the method spiral phase contrast microscopy [15], and for tuning diffractive lenses [16].

At this point, it is relevant to note that conjugated phase refractive elements were suggested for implementing varifocal lenses [17]. This optical procedure adds flexibility when designing nonconventional lens systems [18]. And the same procedure can be suitably translated for designing an optical method that governs the half-width of a Gaussian masks [19].

A pair of refractive, vortex masks are useful for controlling the optical path difference of axicons, lenses and axilenses [20]. Helical filters can be thought of as free-form optical pairs for implementing tunable apodizers [21] and for proposing novel spatial filters [22]; as well as for setting aberration generators in tandem [23] and other types of optical devices [24].

We note that helical phases are related to phase singularities that are implemented by using computer generated holograms [25] and fork gratings [26].

Here, we identify the necessary and the sufficient conditions for controlling the presence of optical vortices. Next, we present two different

sets of optical masks, which are useful for governing the presence of optical vortices. To that end, we employ a pair of transparent masks with helical phase variations. The complex amplitude transmittance of one element, of the proposed pair, is the complex conjugate of the other element. We show that by introducing an in-plane rotation between the elements, of the proposed pairs, one can control the presence of an optical vortex.

For the first set of optical masks, we use transparent masks that have quadratic helical variations. For the second set of optical masks, we employ masks that have cosinusoidal helical phase variations. These results allow us to propose an optical method for detecting angular misalignments.

In Section 2, we use McCutchen theorem [27,28] for relating zero values of the axial irradiance distribution with the zero angular averages over an optical mask. This connection allows us to identify the necessary and sufficient conditions for controlling the presence of an optical vortex. In Section 3, we describe the use of a pair transparent masks, which have quadratic helical variations. In Section 4, we extend our discussion to the use of a pair transparent masks, which have cosinusoidal helical variations. In Section 5, we suggest an application of our previous results, for setting an optical detector that senses angular misalignments. In Section 6, we summarize our contribution.

2. Axial irradiance distribution and angular averages

In Fig. 1 we show the schematics of the optical setup under discussion. In the image plane the cartesian coordinates (x, y, z) are

* Corresponding author.

E-mail address: jojedacas@ugto.mx (J. Ojeda-Castañeda).

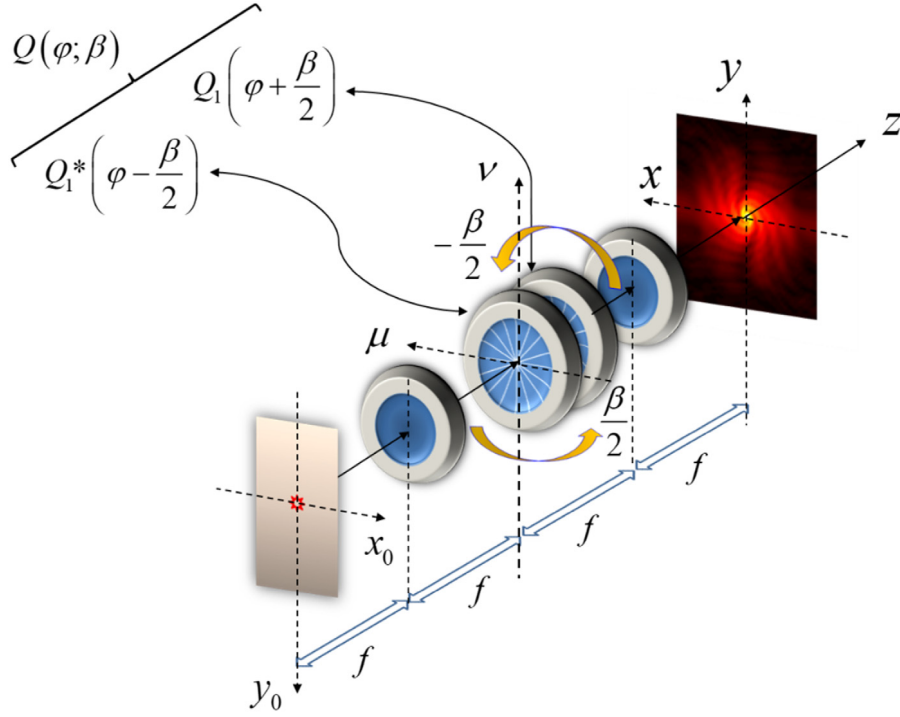


Fig. 1. Schematics of the optical setup for controlling the presence of optical vortices.

expressed as the cylindrical coordinates (r, θ, z) . Next, for describing the use of the optical processor, we evaluate the 3-D complex amplitude point spread function (PSF), $p(r, \theta, z; \beta)$. In our current description, we restrict our discussion to the paraxial regime. That is, for describing the variations beyond the image plane, the generalized pupil function only incorporates a quadratic phase factor. Hence, in the paraxial regime, the PSF is obtained by evaluating the integral

$$p(r, \theta, z; \beta) = \int_0^\Omega \int_0^{2\pi} P(\rho, \varphi; \beta) \times \exp \left\{ i2\pi \left[-\frac{\lambda z}{2} \rho^2 + r \rho \cos(\theta - \varphi) \right] \right\} \rho d\rho d\varphi. \quad (1)$$

In Eq. (1) the Greek letter beta, β , is parameter that represents a rotation angle, at the Fraunhofer plane. At this plane, the polar coordinates are (ρ, φ) . They are here used instead of the spatial frequency, cartesian coordinates (μ, ν) . We can represent a pupil aperture, with maximum radius $\rho = \Omega$, as the circular function

$$\text{circ} \left(\frac{\rho}{\Omega} \right) = \begin{cases} 1 & \text{if } 0 \leq \rho \leq \Omega \\ 0 & \text{if } \rho > \Omega \end{cases}; \quad \rho^2 = \mu^2 + \nu^2. \quad (2)$$

Furthermore, as in the integrand of Eq. (1), we denote as $P(\rho, \varphi; \beta)$ the overall complex amplitude transmittance of the pupil function. That is,

$$P(\rho, \varphi; \beta) = Q(\varphi; \beta) \text{circ} \left(\frac{\rho}{\Omega} \right). \quad (3)$$

In Eq. (3), we denote the complex amplitude transmittance of the pair of transparent masks as

$$Q(\varphi; \beta) = Q_1 \left(\varphi + \frac{\beta}{2} \right) Q_1^* \left(\varphi - \frac{\beta}{2} \right). \quad (4)$$

If we evaluate Eq. (1) along the optical axis, of the system depicted in Fig. 1, we obtain

$$p(0, \theta, z; \beta) = \pi \int_{\rho=0}^{\Omega^2} \left[\frac{1}{2\pi} \int_{\varphi=0}^{2\pi} Q(\varphi; \beta) d\varphi \right] \exp[-i\pi\lambda z \rho^2] d(\rho^2). \quad (5)$$

In Eq. (5), it is convenient to recognize the following angular average

$$\langle Q(\beta) \rangle = \left[\frac{1}{2\pi} \int_{\varphi=0}^{2\pi} Q(\varphi; \beta) d\varphi \right]. \quad (6)$$

Hence, by using Eqs. (5) and (6) we obtain that the normalized, axial irradiance distribution is

$$I(z; \beta) = \frac{|p(0, \theta, z; \beta)|^2}{|\pi\Omega^2|^2} \quad (7)$$

$$I(z; \beta) = |\langle Q(\beta) \rangle|^2 \sin^2 \left(\frac{\lambda\Omega^2 z}{2} \right).$$

From Eq. (7), and as depicted at the left-hand side of Fig. 2, we have the following sufficient condition. If the modulus of the angular average is equal to zero, then the axial irradiance is equal to zero at any value of z . In mathematical terms,

$$\text{If } |\langle Q(\beta) \rangle| = 0 \text{ then } I(z; \beta) = 0. \quad (8)$$

Next, we explore the possibility that Eq. (8) also expresses a necessary condition. To this end, let us assume that there are certain optical masks, which are able to generate zero axial irradiance, but these masks do not have zero angular average. This condition is depicted at the left-hand side of the Venn diagram in Fig. 2; as the existence of a set A_3 .

In mathematical terms, our testing hypothesis is the following

$$\text{If } |\langle Q(\beta) \rangle| \neq 0 \text{ is it possible that } I(z; \beta) = 0? \quad (9)$$

From Eqs. (8) and (9), and from the right-hand side of Fig. 2, we have that if the angular average is different from zero, at $z = 0$, the axial irradiance is also different from zero. Thus, the necessary and sufficient conditions for zero axial irradiance at $z = 0$, is that the angular average must be equal to zero. In mathematical terms,

$$\text{If } |\langle Q(\beta) \rangle| \neq 0 \text{ then } I(z = 0; \beta) \neq 0. \quad (10)$$

And therefore, $I(z; \beta) = 0$ does not necessarily implies $|\langle Q(\beta) \rangle| = 0$. However, $I(z = 0; \beta) = 0$ necessarily implies $|\langle Q(\beta) \rangle| = 0$.

Consequently, in what follows we employ Eqs. (8) and (10) for identifying the presence of an optical vortex, as the necessary and sufficient conditions $I(z = 0; \beta) = 0$.

In a lax manner, one can say that if a phase mask is able to generate a zero angular average, at $z = 0$, then the mask generates an optical vortex.

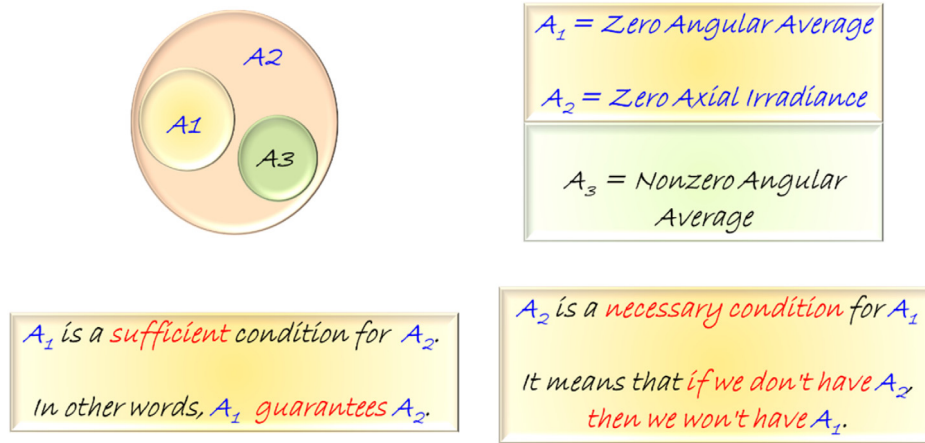


Fig. 2. Venn diagram for illustrating the sufficient and necessary conditions in Eq. (8).

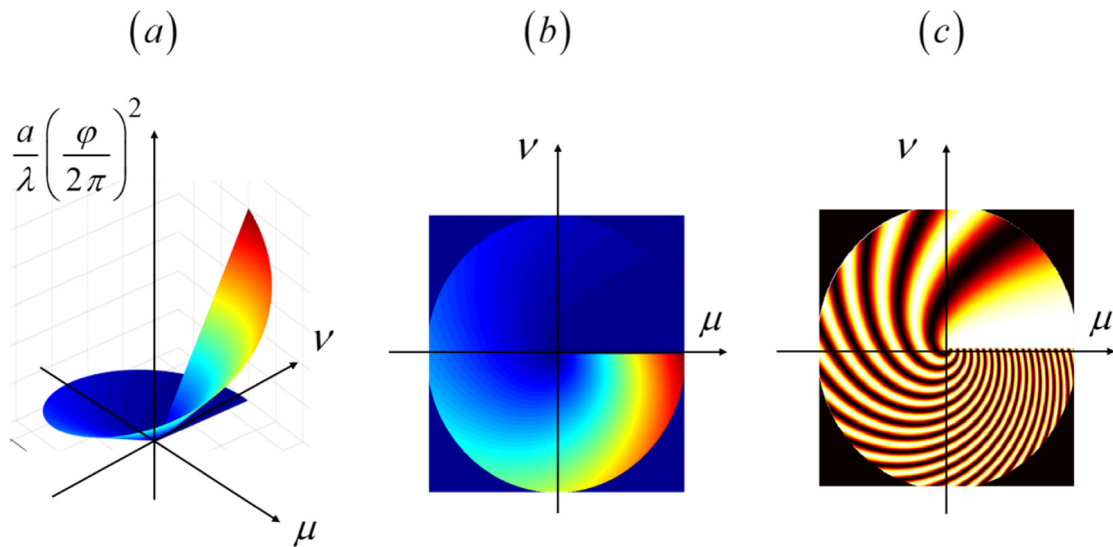


Fig. 3. Quadratic helical phase variations. In (a) we show a 3-D graph. In (b) we depict a 2-D contour plot. And in (c) we display the associated interferogram.

3. Quadratic helical phase variations

Here we consider the use of a pair of transparent masks, each of them has a quadratic helical variation. Then, the complex amplitude transmittance of a single element is

$$Q_1(\varphi) = \exp \left[i2\pi \left(\frac{a}{\lambda} \right) \left(\frac{\varphi}{2\pi} \right)^2 \right]. \quad (11)$$

In Eq. (11), we denote with the lower-case letter “a” the optical path difference of the optical masks; and the Greek letter λ is used for denoting the wave length of the optical radiation. In Fig. 3, we display the phase delay and the interferogram of the transparent profile in Eq. (11).

From Eqs. (4) and (11) we obtain that for the pair of transparent masks, with quadratic helical phase, the overall the complex amplitude transmittance reads

$$Q(\varphi; \beta) = \exp \left[i \left(\frac{a}{\lambda} \beta \right) \left(\frac{\varphi}{2\pi} \right) \right]. \quad (12)$$

The interferogram, between a plane wavefront and the phase delay in Eq. (12), is shown in Fig. 4 for several values of the angle beta.

From Eqs. (6) and (12), it is straightforward to show that $I(z = 0; \beta) = 0$. For further visualizing the influence of the rotation angle β , on Eq. (12), we use polar diagrams in Fig. 5. As a reference phase, we depict a linear helical phase variation as a black, broken curve. After

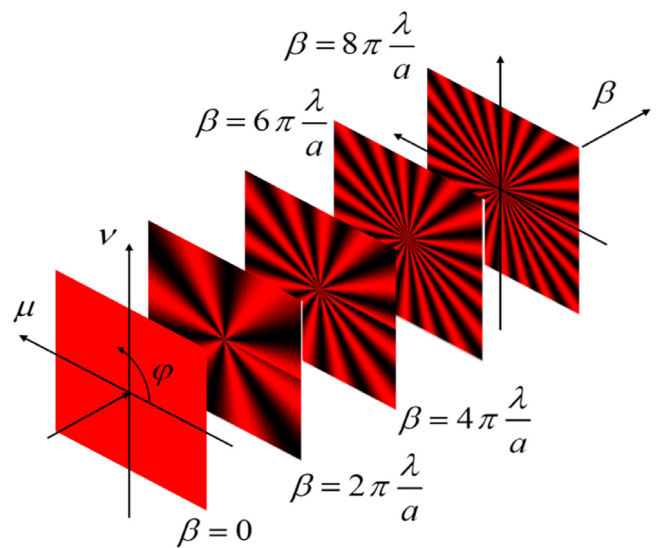


Fig. 4. Irradiance distributions of the interferograms obtained by using a plane wave, as a reference beam, and the phase variations in Eq. (12).

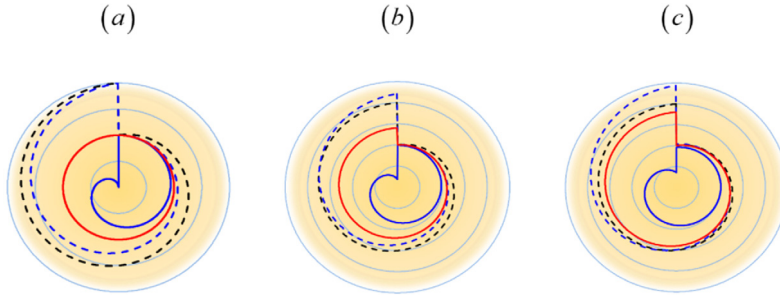


Fig. 5. Polar display of the quadratic, helical phase variations. In (a) $\beta = 0$; in (b) $\beta = \pi/5$; and in (c) $\beta = 2\pi/5$. In broken black lines, we depict a linear helical phase that is used as a reference phase. In broken blue curves, we describe the quadratic helical phase, after introducing a left-hand rotation by an angle $\beta/2$. In continuous blue curves, we depict the phase variations, after introducing a right-hand rotation by an angle $\beta/2$. And the red curves show the overall helical phase.. (For interpretation of the references to color in this figure legend, the reader is referred to the web version of this article.)

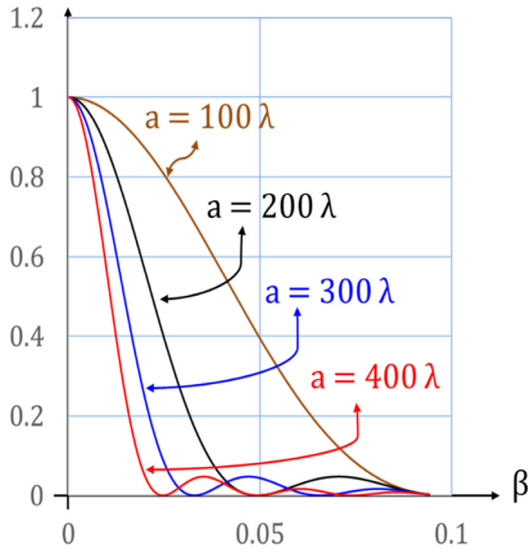


Fig. 6. Graphs of the squared angular averages, as in Eq. (13), for several values of the optical path difference, a (in units of λ).

introducing a left-hand rotation, by an angle $\beta/2$, on the first element of the pair – $Q_1(\varphi + \beta/2)$ in Eq. (11) – the phase changes are depicted in the blue, broken lines. By introducing a right-hand rotation, by an angle $\beta/2$, to the second element of the pair – $Q_1^*(\varphi - \beta/2)$ in Eq. (11) – the phase changes are described by the solid blue lines. The red curves show the overall helical phase delay, caused by the two elements working as a pair.

It is apparent from Fig. 5(a) that for $\beta = 0$, the overall phase (red curve) is equal to zero for any value of the polar angle φ . In Fig. 5(b), we set $\beta = \pi/5$. In this later case, the red curve approaches the reference linear, helical phase; which is depicted with broken black lines. Next, in Fig. 5(c), we set $\beta = 2\pi/5$. Now, the red curve reaches the reference linear, helical phase.

Now, we recognize that by using Eqs. (6) and (12), the squared modulus of the angular average is

$$|\langle Q(\beta) \rangle|^2 = \sin^2 c^2 \left(\frac{a}{\pi \lambda} \beta \right). \quad (13)$$

In Fig. 6, we plot the square values of the angular average, in Eq. (13), for several values of the optical path differences.

Thus, from Eq. (13) and Fig. 6, we have that for generating an optical vortex the condition is

$$\beta = m \frac{\lambda}{a} \pi; \quad \text{for } m = \pm 1, \pm 2, \dots \quad (14)$$

For many practical applications, we note that for thick optical masks with $a = 3000 \lambda$, the angular increments are equal to $\Delta\beta = \pi / 3000 (=$

$0.03^\circ)$, which is indeed a rather small rotation angle. This value maybe useful for detecting small rotations between the elements of a pair. Of course, this high sensitivity is reduced for a transparent element with masks that have a path difference of $a = 300 \lambda$. Then, one can generate an optical vortex with angular increments of $\Delta\beta = \pi / 300 (= 0.3^\circ)$.

In Fig. 7, we show the irradiance PSF's that are generated by using the propose quadratic helical phase elements, as a pair. In Fig. 7(a) we have that $\beta = 0$. In Fig. 7(b) we set $\beta = \pi/200$. And in Fig. 7(c), $\beta = \pi/50$.

It is apparent from Fig. 7 that indeed, one can control the presence of an optical vortex by introducing an in-plane rotation between the elements of the proposed pair. Next, we analyze another possibility for governing an optical vortex.

4. Cosinusoidal helical phase variations

Now, we consider the use of a pair of transparent masks with cosinusoidal helical phase variations. In this case, the complex amplitude transmittance of a single element is

$$Q_2(\varphi) = \exp \left[i2\pi \left(\frac{a}{\lambda} \right) \cos(\varphi) \right]. \quad (15)$$

In Eq. (15), we denote again with “ a ” the optical path difference; and the Greek letter λ denotes the wave length of the optical radiation.

In Fig. 8(a), we plot, as a 3-D graph, the cosinusoidal helical phase variations in Eq. (15). In Fig. 8(b), we show a contour map of the same helical phase variations. And in Fig. 8(c), we display the interferogram of the proposed phase.

From Eqs. (4) and (15) we have that the overall complex amplitude transmittance is

$$Q(\varphi) = \exp \left[-i2\pi \left(\frac{a}{\lambda} \sin \left(\frac{\beta}{2} \right) \right) \sin(\varphi) \right]. \quad (16a)$$

In Fig. 9 we plot the variations of the phase delay in Eq. (16a), which is expressed as

$$\psi(\varphi; \beta) = \left(\frac{a}{\lambda} \right) \sin \left(\frac{\beta}{2} \right) \sin(\varphi). \quad (16b)$$

The diagram in Fig. 9a is a plot in Cartesian coordinates (φ, ψ) , for $a = 100 \lambda$; and for three different values of the rotation angle beta. The diagram Fig. 9b is a plot in polar coordinates (ψ, φ) , again with $a = 100 \lambda$; and few set $\beta = \pi/10$, $\beta = \pi/5$, and for $\beta = \pi/2$.

As in the previous section, for visualizing the influence of the rotation angle beta, in Fig. 10 we use polar diagrams. In black broken lines, as a reference phase, we depict a sinusoidal helical phase variation. Then, after introducing a left-hand rotation, by an angle $\beta/2$, to the first element of the pair – $Q_2(\varphi + \beta/2)$ as in Eq. (15) – the phase changes are depicted in blue, broken lines. By introducing a right-hand rotation, by an angle $\beta/2$, to the second element of the pair – $Q_2^*(\varphi - \beta/2)$ as in Eq. (15) – the phase changes are described by the solid blue lines. The red curves show the overall helical phase, caused by using the pair of cosinusoidal helical phase masks.

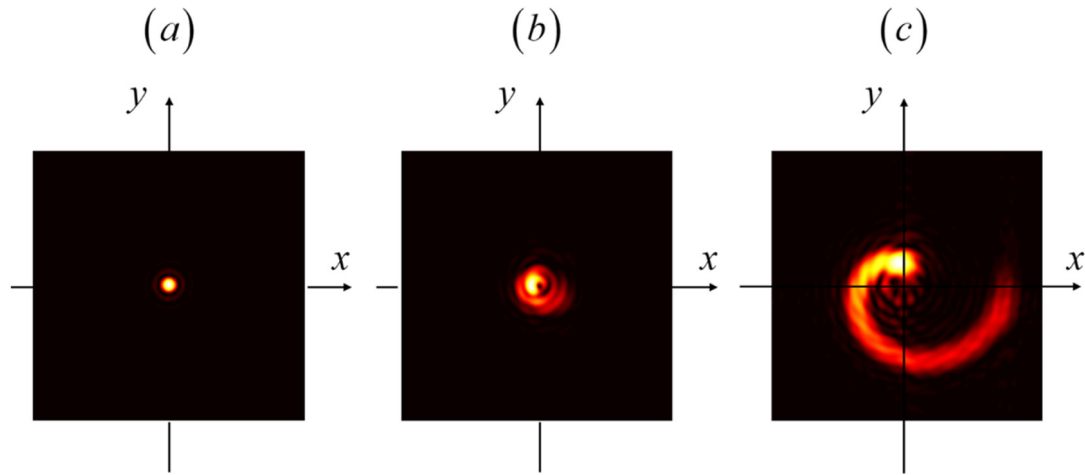


Fig. 7. Irradiance PSFs when using a pair of quadratic helical phase elements, with optical path difference $a = 300 \lambda$. In (a) the rotation angle is $\beta = 0$, in (b) the rotation angle is $\beta = \pi/200$, and in (c) $\beta = \pi/50$.

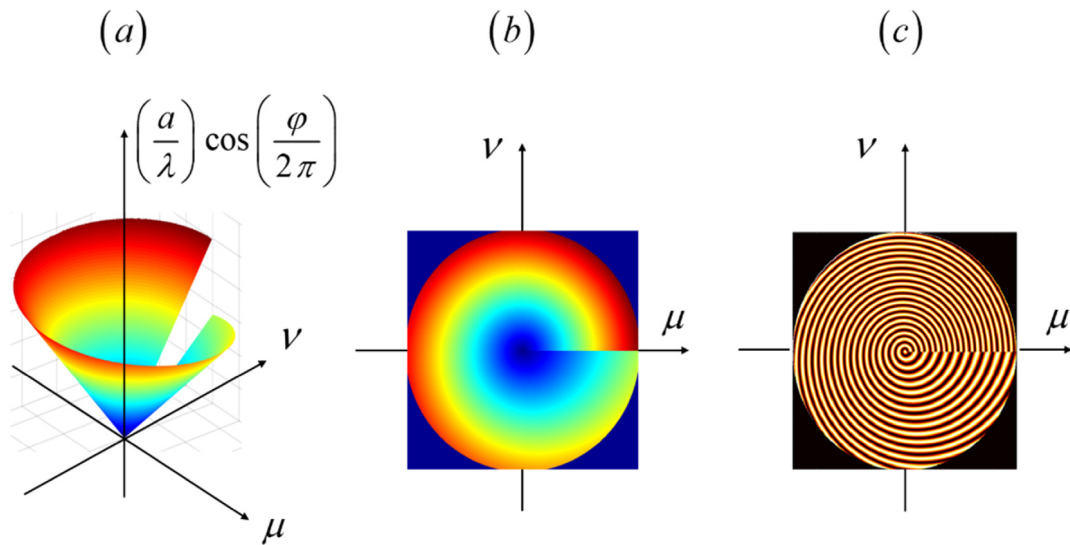


Fig. 8. Cosinusoidal helical masks for an optical path difference $a = 20 \lambda$. In (a) we show a 3-D plot of the cosinusoidal, helical phase variations; in (b) we display a contour graph of the same phase distribution; and in (c) we show the associated interferogram.

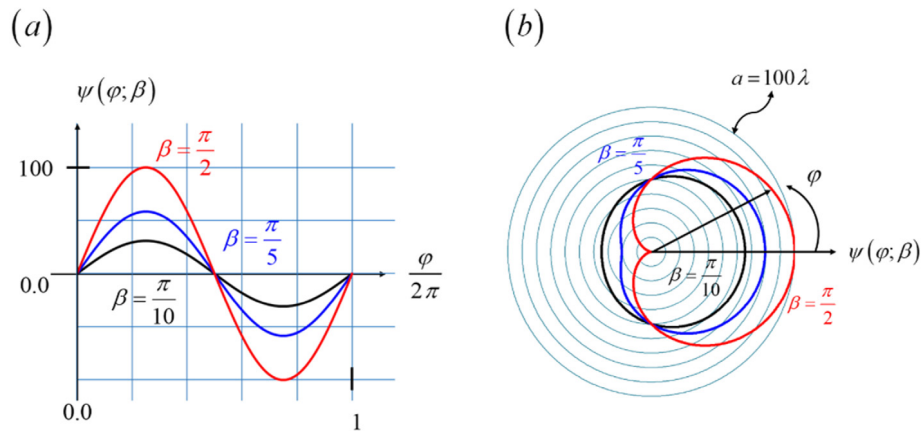


Fig. 9. Phase delays, as in Eq. (16b), for both Cartesian coordinates (φ, ψ) and for polar coordinates (ψ, φ) . We set $a = 100 \lambda$; in black lines $\beta = \pi/10$, in blue lines $\beta = \pi/5$, and in red lines $\beta = \pi/2$. (For interpretation of the references to color in this figure legend, the reader is referred to the web version of this article.)

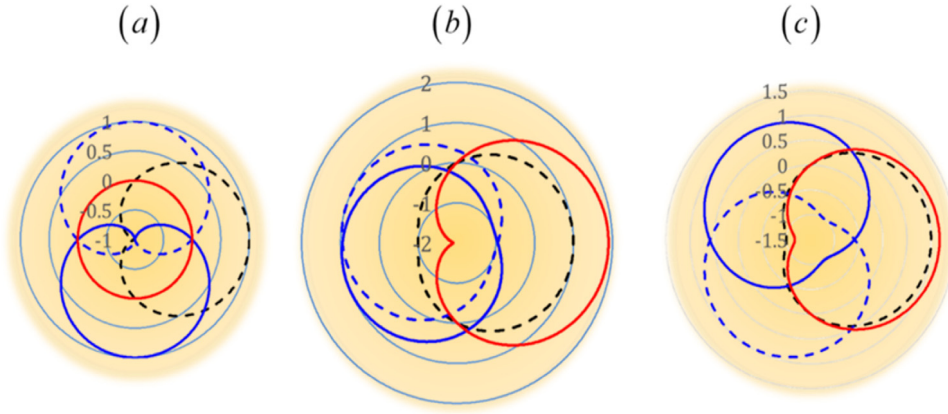


Fig. 10. Polar displays of the cosinusoidal helical phase variations. As a reference phase, in broken black lines, we depict a sinusoidal helical phase. In broken blue lines, we show a cosinusoidal helical phase, after a left-hand rotation by an angle $\beta/2$. In continuous blue lines, we describe the cosinusoidal helical phase variations, after a right-hand rotation by an angle $\beta/2$. And in red curves we display the overall helical phase delay, caused by the pair of elements; each of them with a cosinusoidal helical phase. In (a) $\beta = 0$; in (b) $\beta = \pi/5$; and in (c) $\beta = 2\pi/5$. (For interpretation of the references to color in this figure legend, the reader is referred to the web version of this article.)

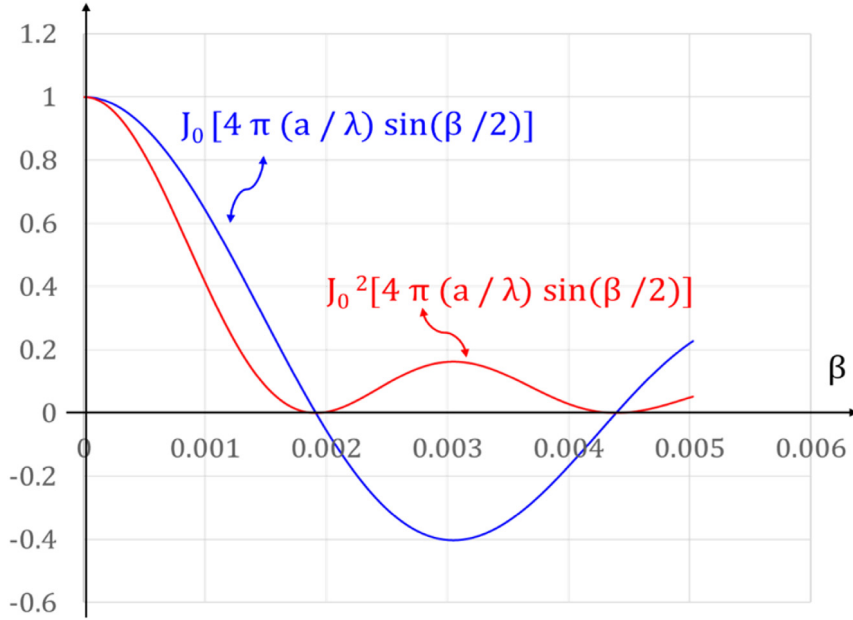


Fig. 11. Graphs of the Bessel function, of the first kind and zero order, and its square values; as in Eq. (17). We set the optical path $a = \lambda/200$.

In Fig. 10(a), we set $\beta = 0$. Then, for any value of the polar angle φ , the overall phase (red curve) is equal to zero. In Fig. 10(b), $\beta = \pi/5$, we note that the red curve starts to follow a path that is similar to the sinusoidal, helical phase in broken black lines. And as depicted in Fig. 10(c), for $\beta = 2\pi/5$, the red curve nears the sinusoidal, helical phase in broken black lines.

Next, we recognize the conditions for governing the presence of an optical vortex. It is straightforward to show from Eqs. (7) and (16a) that

$$|\langle Q(\beta) \rangle|^2 = J_0^2 \left[4\pi \left(\frac{a}{\lambda} \right) \sin \left(\frac{\beta}{2} \right) \right]. \quad (17)$$

In Eq. (17) $J_0(\cdot)$ represents the Bessel function of the first kind, and zero order. In Fig. 11, as blue curve, we display the changes of the Bessel function, of the first kind and zero order, by setting the optical path $a = \lambda/200$. Also, in Fig. 11, we depict the function in Eq. (17). The graphs show that the zero crossing, of the curves, do occur at rather small values of the rotation angle β . Hence, the presence of zero axial irradiance maybe used for evaluating rotation angles.

If we denote the zero crossings, of the Bessel function of zero order, as

$$\sigma_m = \{2.4048, 5.5198, 8.6537, \dots\} \quad (18)$$

then for generating an optical vortex one requires that

$$\beta = 2 \arcsin \left(\frac{\lambda}{4\pi a} \sigma_m \right). \quad (19)$$

Hence, if $a = 300 \lambda$, for generating an optical vortex the first value of the rotation angle is $\beta = 1/500$; and the second value of the rotation angle is $\beta = 4.4/100$. In Fig. 12, we show the irradiance PSF's, which are generated by using the propose cosinusoidal helical phase elements; working as a pair, for $\beta = 0$, $\beta = \pi/100$ and $\beta = \pi/50$, respectively.

From Fig. 12, it is apparent that one can govern the presence of an optical vortex by controlling the in-plane rotations of a pair, of cosinusoidal helical phase masks. In what follows, we apply the previous results for designing an optical sensor of in-plane rotations.

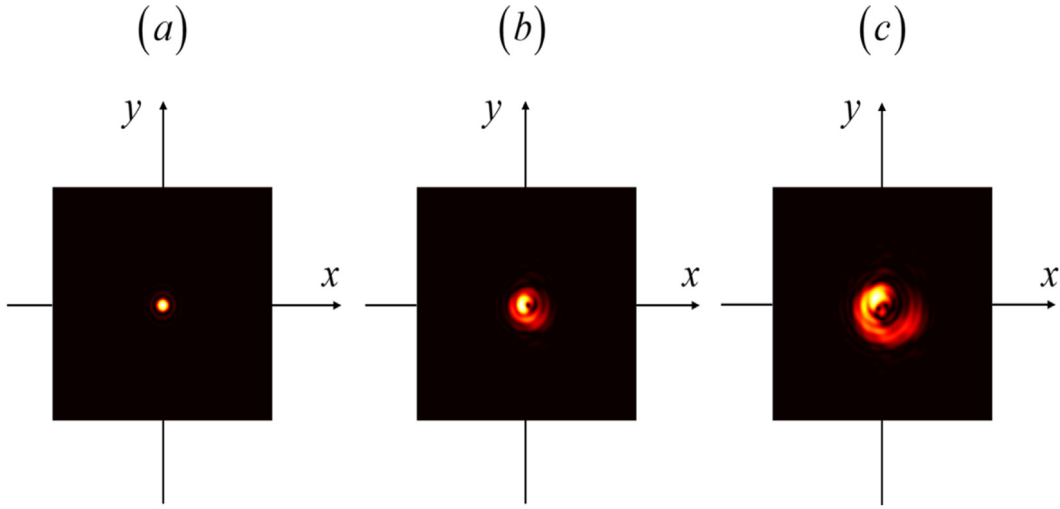


Fig. 12. Point spread functions when using a pair of cosinusoidal helical phase elements, with optical path difference $a = 300 \lambda$. In (a) $\beta = 0$; in (b) $\beta = \pi/100$; and in (c) $\beta = \pi/50$.

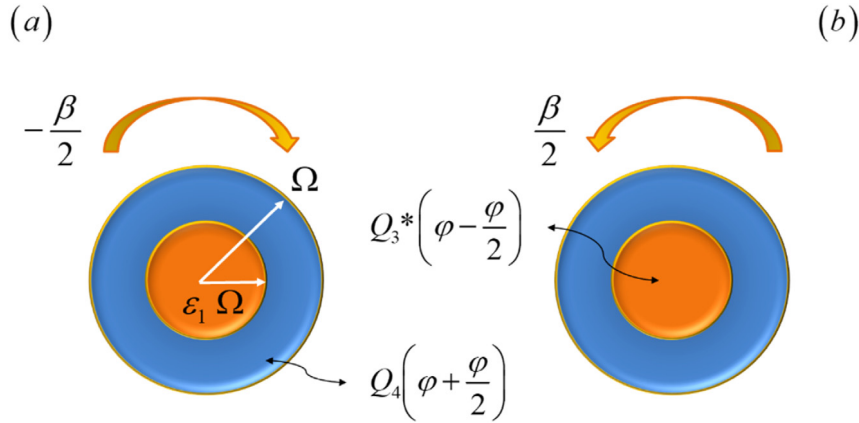


Fig. 13. Sketches showing the composition of two annular regions, which can be rotated independently. Since each annulus has a different optical path difference, they are here depicted in two different colors.. (For interpretation of the references to color in this figure legend, the reader is referred to the web version of this article.)

5. Detection of angular misalignments

As depicted in Fig. 13, we consider now that each member (of a helical pair) has two annular sections; which can in-plane rotate independently.

For the first element of the pair, the complex amplitude transmittance at the first annulus is

$$P_3(\rho, \varphi; \varepsilon) = \text{circ}\left(\frac{\rho}{\varepsilon\Omega}\right) Q_3(\varphi). \quad (20)$$

In Eq. (20) we take into account a reduction in the radius of the inner disk as follows. We denote with the Greek letter ε , a real positive number that is less than unity. That is $0 < \varepsilon < 1$. Then, in Eq. (20) the maximum value of the radius is reduced from Ω to $\varepsilon\Omega$. In accordance to Eq. (2), we have that

$$\text{circ}\left(\frac{\rho}{\varepsilon\Omega}\right) = \begin{cases} 1 & \text{if } 0 \leq \rho \leq \varepsilon\Omega \\ 0 & \text{if } \rho > \varepsilon\Omega. \end{cases} \quad (21)$$

Now, by using Eq. (21) we have that at the outer annulus, of the first element of the pair, the complex amplitude transmittance is

$$P_4(\rho, \varphi; \varepsilon) = \left[\text{circ}\left(\frac{\rho}{\Omega}\right) - \text{circ}\left(\frac{\rho}{\varepsilon\Omega}\right) \right] Q_4(\varphi). \quad (22)$$

Hence, by taking into account the contribution of the inner disk and that of the outer disk, the first mask has the following complex amplitude transmittance is

$$P(\rho, \varphi; \varepsilon) = \text{circ}\left(\frac{\rho}{\varepsilon\Omega}\right) Q_3(\varphi) + \left[\text{circ}\left(\frac{\rho}{\Omega}\right) - \text{circ}\left(\frac{\rho}{\varepsilon\Omega}\right) \right] Q_4(\varphi). \quad (23)$$

As in the previous sections, the complex amplitude transmittance of the second mask is the complex conjugate of Eq. (23).

Next, we form a pair by placing the first mask in close contact with the second mask. After introducing an in-plane rotation, say by an angle β , between the masks the overall complex amplitude transmittance is

$$\begin{aligned} P\left(\rho, \varphi + \frac{\beta}{2}; \varepsilon\right) P^*\left(\rho, \varphi - \frac{\beta}{2}; \varepsilon\right) &= \text{circ}\left(\frac{\rho}{\varepsilon\Omega}\right) Q_3\left(\varphi + \frac{\beta}{2}\right) Q_3^*\left(\varphi - \frac{\beta}{2}\right) \\ &+ \left[\text{circ}\left(\frac{\rho}{\Omega}\right) - \text{circ}\left(\frac{\rho}{\varepsilon\Omega}\right) \right] Q_4\left(\varphi + \frac{\beta}{2}\right) Q_4^*\left(\varphi - \frac{\beta}{2}\right). \end{aligned} \quad (24)$$

For this new pair the complex amplitude distribution along the optical axis, in Eq. (7), becomes

$$\begin{aligned} p(0, \theta, z; \beta) &= \pi \varepsilon^2 \Omega^2 \exp\left(-i \frac{\pi \varepsilon^2 \Omega^2}{2} \lambda z\right) \text{sinc}\left(\frac{\varepsilon^2 \Omega^2}{2} \lambda z\right) \langle Q_3(\beta) \rangle \\ &+ \pi (1 - \varepsilon^2) \Omega^2 \exp\left(-i \frac{\pi (1 + \varepsilon^2) \Omega^2}{2} \lambda z\right) \\ &\times \text{sinc}\left(\frac{(1 - \varepsilon^2) \Omega^2}{2} \lambda z\right) \langle Q_4(\beta) \rangle. \end{aligned} \quad (25)$$

In Eq. (25) the functions of β are the angular averages $\langle Q_3(\beta) \rangle$ and $\langle Q_4(\beta) \rangle$. Consequently, by assuming that $\langle Q_3(\beta) \rangle$ and $\langle Q_4(\beta) \rangle$ are real functions, the normalized axial irradiance distribution is

$$I(z; \beta) = \varepsilon^4 \sin^2 c^2 \left(\frac{\lambda \varepsilon^2 \Omega^2}{2} z \right) |\langle Q_3(\beta) \rangle|^2 + (1 - \varepsilon^2)^2 \sin^2 c^2 \left(\frac{\lambda(1 - \varepsilon^2) \Omega^2}{2} z \right) |\langle Q_4(\beta) \rangle|^2 + 2\varepsilon^2 (1 - \varepsilon^2)^2 \sin^2 c \left(\frac{\lambda \varepsilon^2 \Omega^2}{2} z \right) \times \sin c \left(\frac{\lambda(1 - \varepsilon^2) \Omega^2}{2} z \right) \langle Q_3(\beta) \rangle \langle Q_4(\beta) \rangle. \quad (26)$$

It is clear from Eq. (26) that if the two angular averages are zero, then we have an optical vortex. In particular, if the two annular regions have quadratic helical phase variations, the condition reads

$$\langle Q_3(\beta) \rangle = 0 = \sin^2 c^2 \left(\frac{a_1}{\pi \lambda} \beta \right) \langle Q_4(\beta) \rangle = 0 = \sin^2 c^2 \left(\frac{a_2}{\pi \lambda} \beta \right). \quad (27)$$

As before, in Eq. (27) the lower-case Latin letters a_1 and a_2 stand for the optical path differences of each quadratic, helical phase. Admittedly, the result in Eq. (27) accepts other possibilities. However, these other possibilities are outside our current scope. Next, we apply the result in Eq. (27).

Let us consider that the inner annulus has an optical path with twice the value of the outer annulus. In mathematical terms, if $a_1 = 2a_2 = 400\lambda$. Then, one could switch-on a vortex if the rotation angle, of the inner annulus, is $\beta_m = m \frac{\pi}{400}$. And, one could switch-on a vortex if the rotation angle, of the outer annulus, is $\beta_n = n \frac{\pi}{200}$. Both requirements are satisfied if one selects $m = 2$ and $n = 1$.

Thus, for obtaining a zero-irradiance value at the optical axis, the rotation angle of the inner annulus must be twice the value of the rotation angle of the outer annulus.

This strong simultaneous condition can be used in two stages test. First, the outer annulus is rotated by an angle $\beta_2 = \frac{\pi}{200}$. Second, for verifying the correctness of β_2 , one needs to rotate the inner disk by an angle $\beta_1 = \frac{\pi}{400}$. If both values are right, then an axial irradiance with zero value verifies the correctness of the rotation angles.

6. Final remarks

We have discussed the necessary and the sufficient conditions for controlling the presence of optical vortices. Along our discussion, we have unveiled the use of two different pairs of helical phase masks, which can govern the presence of an optical vortex.

We have stated that the complex amplitude transmittance of one element, of the proposed pair, is the complex conjugate of the other element. Then, we have shown that one can control the presence of an optical vortex, by introducing an in-plane rotation, say by an angle β , between the elements of the pair.

We have identified two suitable pairs of helical phase masks. The first set, the elements of the pair have quadratic helical variations. In the second set, the elements of the pair have sinusoidal helical phase variations.

In both cases, we have associated the presence of an optical vortex as the capability of generating zero irradiance, at $z = 0$ on the optical axis of an optical processor. We have reported two analytical formulas that describe the production of zero axial irradiance, in terms of the rotation angle β .

The reported formulas are useful for identifying suitable optical path difference and suitable rotation angles, for generating an optical vortex. We have evaluated numerically some PSF, of the proposed pairs, for verifying that one can control the presence on an optical vortex.

Finally, we have described an optical device that senses angular misalignments. This novel device uses elements with helical phase, over two independent annular regions. Each annular region has a different optical path difference. We have reported an analytical formulation of this proposal, which describes the use of a pair of masks over two annular regions, for double checking the value of the rotation angle beta.

Declaration of competing interest

The authors declare that they have no known competing financial interests or personal relationships that could have appeared to influence the work reported in this paper.

Acknowledgments

We would like to thank the reviewers for their thorough job in identifying mistakes, as well as for suggesting valuable amendments.

References

- [1] James Dyson, Circular and spiral diffraction gratings, Proc. R. Soc. Lond. Ser. A Math. Phys. Eng. Sci. 248 (1958) 93–106.
- [2] J.F. Nye, M.V. Berry, Dislocations in wave trains, Proc. R. Soc. Lond. Ser. A Math. Phys. Eng. Sci. 336 (1974) 65–190.
- [3] Guy Indebetouw, Optical vortices and their propagation, J. Modern Opt. 40 (1993) 73–87.
- [4] M.W. Beijersbergen, R.P.C. Coerwinkel, M. Kristensen, J.P. Woerdman, Helical wavefront laser beams produced with a spiral phase plate, Opt. Commun. 112 (1994) 321–327.
- [5] D.G. Grier, A revolution in optical manipulation, Nature 424 (2003) 810–816.
- [6] S.S.R. Oemrawsingh, J.A.W. van Houwelingen, E.R. Eliel, J.P. Woerdman, E.J.K. Verstege, J.G. Kloosterboer, G.W. 't Hooft, Production and characterization of spiral phase plates for optical wavelengths, Appl. Opt. 43 (2004) 688–694.
- [7] Olof Bryngdahl, Radial- and circular-fringe interferograms, J. Opt. Soc. Amer. 63 (1973) 1098–1104.
- [8] S. Fühapter, A. Jesacher, S. Bernet, M. Ritsch-Marte, Spiral interferometry, Opt. Lett. 30 (2005) 1953–1955.
- [9] V.V. Kotlyar, A.A. Almazov, S.N. Khonina, V.A. Soifer, H. Elfstrom, J. Turunen, Generation of phase singularity through diffracting a plane or Gaussian beam by a spiral phase plate, J. Opt. Soc. Amer. A 22 (2005) 849–861.
- [10] Alison M. Yao, Miles J. Padgett, Orbital angular momentum: origins, behavior and applications, Adv. Opt. Photon. 3 (2011) 161–204.
- [11] A.W. Lohmann, J. Ojeda-Castañeda, N. Streibl, Spatial periodicities in coherent and partially coherent fields, Opt. Acta 30 (1983) 1259–1266.
- [12] P. Szwaykowski, J. Ojeda-Castañeda, Nondiffracting beams and the self-imaging phenomenon, Opt. Commun. 83 (1991) 1–4.
- [13] J. Ojeda-Castaneda, Pedro Andrés, Manuel Martínez-Corral, Zero axial irradiance by annular screens with angular variation, Appl. Opt. 31 (1992) 4600–4602.
- [14] Gregory Foo, David M. Palacios, Grover A. Swartzlander Jr., Optical vortex coronagraph, Opt. Lett. 30 (2005) 3308–3310.
- [15] S. Bernet, A. Jesacher, S. Fühapter, C. Maurer, M. Ritsch-Marte, Quantitative imaging of complex samples by spiral phase contrast microscopy, Opt. Express 14 (2006) 3792–3805.
- [16] S. Bernet, M. Ritsch-Marte, Optical device with a pair of diffractive optical elements, U.S. patent application 20100134869 A1, 2010.
- [17] A.W. Lohmann, A new class of varifocal lenses, Appl. Opt. 9 (1970) 1669–1671.
- [18] J. Ojeda-Castañeda, C.M. Gómez-Sarabia, Nonconventional optical systems using varifocal lenses, Phot. Lett. Poland 7 (2015) 14–16.
- [19] J. Ojeda-Castañeda, E. Yépez-Vidal, E. García-Almanza, C.M. Gómez-Sarabia, Tunable Gaussian mask for extending the depth of field, Phot. Lett. Poland 4 (2012) 115–117.
- [20] J. Ojeda-Castañeda, Cristina M. Gómez-Sarabia, Sergio Ledesma, Tunable focalizers: axicons, lenses and axilenses, Proc. Soc. Photo-Opt. Instrum. Eng. 8833 (2013) 883306_1-883306_6.
- [21] J. Ojeda-Castañeda, Sergio Ledesma, Cristina M. Gómez-Sarabia, Tunable apodizers and tunable focalizers using helical pairs, Phot. Lett. Poland 5 (2013) 20–22.
- [22] J. Ojeda-Castañeda, Cristina M. Gómez-Sarabia, Sergio Ledesma, Novel free-form optical pairs for tunable focalizers, J. Opt. (India) 43 (2014) 85–91.
- [23] J. Ojeda-Castaneda, Ana L. Barragán-Chávez, Cristina M. Gómez-Sarabia, Aberration generators in tandem, Phot. Lett. Poland 7 (2015) 8–10.
- [24] Jorge Ojeda-Castañeda, Cristina M. Gómez-Sarabia, Tunable focalizers: phase conjugate pairs, in: Proc. Soc. Photo-Opt. Instrum. Eng., 2019, 112072, 112072_L1-112072_L10.

- [25] A. Vasara, J. Turunen, A.T. Friberg, Realization of general nondiffracting beams with computer-generated holograms, *J. Opt. Soc. Amer. A* 6 (1989) 1748–1754.
- [26] N.R. Heckenberg, R. McDuff, C.P. Smith, A.G. White, Generation of optical phase singularities by computer generated holograms, *Opt. Lett.* 17 (1992) 221–223.
- [27] C.W. McCutchen, Generalized aperture and the three-dimensional diffraction image, *J. Opt. Soc. Amer.* 54 (1964) 240.
- [28] J. Ojeda-Castañeda, Cristina M. Gómez-Sarabia, Tuning field depth at high resolution by pupil engineering, *Adv. Opt. Photon.* 7 (2015) 814–880.